








Spin-orbit interaction in nanofiber-based Brillouin scattering

MAXIME ZERBIB,^{1,*}  MAXIME ROMANET,¹ 
THIBAUT SYLVESTRE,¹  CHRISTIAN WOLFF,² 
BIRGIT STILLER,^{3,4} JEAN-CHARLES BEUGNOT,¹ 
AND KIEN PHAN HUY^{1,5}

¹FEMTO-ST Institute, UMR 6174 CNRS-Université de Franche-Comté, 25030 Besançon, France

²Center for Nano Optics, University of Southern Denmark, Campusvej 55, DK-5230 Odense M, Denmark

³Max Planck Institute for the Science of Light, Staudtstr. 2, 91058 Erlangen, Germany

⁴Department of Physics, University of Erlangen-Nuremberg, Staudtstr. 7, 91058 Erlangen, Germany

⁵SUPMICROTECH-ENSM, 25000 Besançon, France

*maxime.zerbib@femto-st.fr

Abstract: Angular momentum is an important physical property that plays a key role in light-matter interactions, such as spin-orbit interaction. Here, we investigate theoretically and experimentally the spin-orbit interaction between a circularly polarized optical (spin) and a transverse vortex acoustic wave (orbital) using Brillouin backscattering in a silica optical nanofiber. We specifically explore the state of polarization of Brillouin backscattering induced by the TR21 torso-radial vortex acoustic mode that carries an orbital angular momentum. Using a full-vectorial theoretical model, we predict and observe two operating regimes for which the backscattered Brillouin signal is either depolarized or circularly polarized, depending on the input pump polarization. We demonstrate that when the pump is circularly polarized and thus carries a spin angular momentum, the backscattered signal undergoes a handedness reversal of circular polarization due to opto-acoustic spin-orbit interaction and the conservation of overall angular momentum.

© 2023 Optica Publishing Group under the terms of the [Optica Open Access Publishing Agreement](#)

1. Introduction

Spin-orbit interaction (SOI), whereby spin and orbital features of a particle or a wave affect each other, is a striking and ubiquitous phenomenon occurring in many fields of physics, such as solid-state and quantum physics, optics, and acoustics. In optics, it has long been known that light carries both orbital angular momentum (OAM) and spin angular momentum (SAM), related to wavefront rotation and circular polarization, respectively, and that they can become coupled by SOI while conserving the overall angular momentum [1,2]. As early as 1909, Poynting suggested that circularly polarized light possesses a SAM known as the spin of light [3]. The conservation of angular momentum in an optomechanical interaction was then experimentally evidenced in 1936 by Beth [4], who showed that the conversion of left-handed circular polarization to right-handed circular polarization through a crystalline waveplate induces an opposite torque on the waveplate. This pioneering experiment still resonates in the scientific community today, as shown by numerous studies over the past decades in optical tweezers and other applications based on SOI [5–8]. Although this effect attracts interest beyond optics [9], it is at the heart of many studies in photonics [1,2] with major applications in the manipulation of small objects and light itself [10]. The coupling between light SAM and OAM can give rise to intriguing phenomena such as photonic spin-Hall effect [11,12] and spin-dependent vortex generation [13]. In acoustics, SOI has recently been reported using elastic spin and angular momenta of transverse acoustic beams [14,15].

In this paper, we report an optoacoustic spin-orbit interaction using Brillouin backscattering in a silica optical nanofiber [16–18], whereby a circularly polarized optical mode carrying a SAM coherently interacts with a torso-radial (TR21) vortex acoustic mode that has non-zero OAM. We show in particular that the backscattered Brillouin signal by the TR21 acoustic mode has an opposite circular polarization due to the spin-orbit coupling and the conservation of total angular momentum. Our observations complete other recent studies about optoacoustic angular momentum conservation and polarization effects in other fiber types, such as chiral photonic crystal fibers [19–21], standard single-mode fibers [22–24], and multimode fibers [25]. They are relevant not only for further fundamental investigations but also for several applications, such as new distributed sensing schemes based on SOIs, nonreciprocal isolating devices [19], or Brillouin-based optical memories using the polarization inversion of backscattered light as an additional degree of storage [26,27].

The paper is organized as follows. In the first section, we describe the theoretical background of Brillouin light backscattering by the TR21 acoustic vortex wave in an optical nanofiber. We then show that, when the incident light is linearly polarized, we observe a polarization scrambling of the scattered light similar to previous forward Brillouin scattering experiments [28]. On the other hand, when the pump light is circularly polarized and therefore has a SAM, the SOI allows the backscattered light to be fully polarized with handedness reversal. In the second and third sections, we present experimental polarization-sensitive measurements of Brillouin backscattering in a 730-nm diameter silica nanofiber, and we confirm our theoretical predictions.

2. Principle and theory

Figure 1(a) schematically illustrates the Brillouin backscattering in a tapered optical nanofiber (ONF), which results from the coherent interaction between an optical pump wave depicted in blue and an acoustic wave (in purple). This optoacoustic interaction gives rise to an optical backscattered Stokes wave (in red) which is shifted in frequency from a few GHz due to the Doppler effect. It is governed by both energy conservation as $\omega_a = \omega_p - \omega_s$ (a =acoustic, p =pump, s =Stokes), and momentum conservation with a phase-matching condition that reads as $\beta_a = \beta_p - \beta_s$ where $(\omega_i, \beta_i)_{i \in \{a,p,s\}}$ are the angular frequencies and propagation constants, respectively. Unlike standard optical fibers, in sub-wavelength fibers, Brillouin backscattering has been shown to rely on several hybrid acoustic modes, including longitudinal, radial, torso-radial, and surface modes [17,18]. Among those acoustic modes, the torso-radial TR21 one is characterized by scalar potential and vector potential components with an azimuthal order 2, as shown in Figs. 1(b)–(e) (for details, see Supplement 1, Note 1). However, since sub-wavelength optical fibers exhibit a slight ellipticity due to their manufacturing process based on the tapering of standard single-mode fibers [29], the TR21 acoustic mode can be decomposed into two degenerated modes, which are denoted TR21_× and TR21₊ in Figs. 1(b) and (c). These two modes can also linearly be combined to two other vortex TR21_⊙ and TR21_⊙ modes (Figs. 1(d) and (e), as in-phase and quadrature standing waves, with a topological charge $l = \pm 2$ (Supplement 1, Note 1).

To model the optoacoustic Brillouin interaction between the pump and these two acoustic modes, we used the wave equations driven by the electrostrictive stress, which can be written as [30–32]:

$$\rho \frac{\partial^2 u_i}{\partial t^2} + \eta_{ij} \frac{\partial u_j}{\partial t} - c_{ijkl} \frac{\partial^2 u_l}{\partial x_k \partial x_j} = -\chi_{klj} \epsilon_0 \frac{\partial}{\partial x_j} E_k^{(P)} E_l^{(S)*} \quad (1)$$

$$\nabla^2 E_j^{(S)} - \frac{1}{c^2} \epsilon_r \frac{\partial^2 E_j^{(S)}}{\partial t^2} = \chi_{jlim} \frac{2}{c^2} \frac{\partial^2 E_j^{(P)}}{\partial t^2} \left(\frac{\partial u_i^*}{\partial x_m} \right) \quad (2)$$

where ρ is the silica material density, u_i is the displacement field components in three-dimensional space ($i \in \{x, y, z\}$), c_{ijkl} are the elastic tensor components. The index following a comma stands

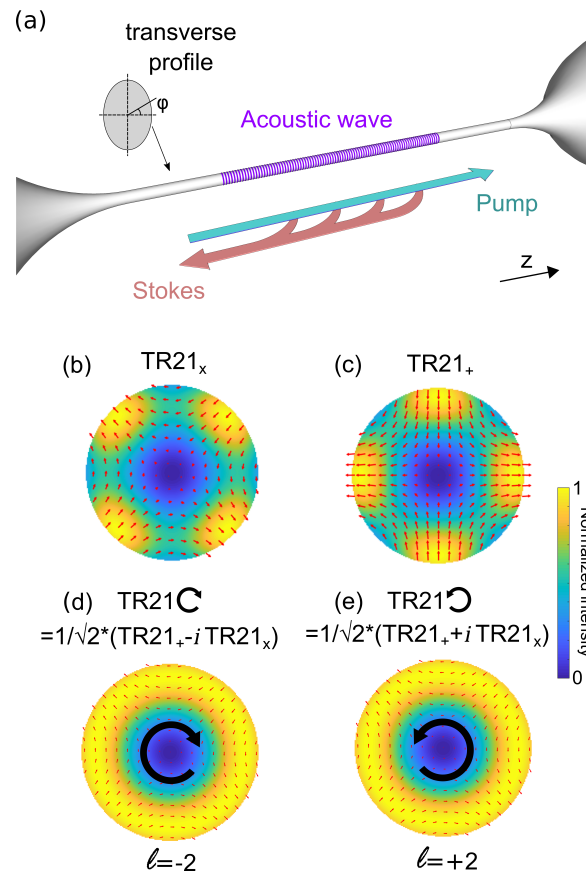


Fig. 1. (a) Illustration of Brillouin backscattering in a tapered optical nanofiber. (b) and (c) are the $TR21_x$ and $TR21_+$ degenerated stationary torso-radial modes assuming a slight elliptical core. The red arrows show the transverse displacement field and the false colors show the normalized transverse kinetic energy. (d) and (e) are the vortex acoustic modes $TR21 \odot$ and $TR21 \ominus$ resulting from the sum of the two previous stationary modes $\mp\pi/2$ -shifted. (See Visualization 1, Visualization 2, Visualization 3 and Visualization 4 for animated figures (b), (c), (d) and (e), respectively.)

for the partial derivative with respect to that coordinate. η_{ij} are the viscosity constants, χ_{kilj} is the electrostrictive tensor, ϵ_0 and ϵ_r are the vacuum and relative permittivity respectively. $E_k^{(p)}$ denotes the k-component of the optical pump electric field, $E_l^{(s)}$ being the l-component of the electric field of the optical Stokes signal, and c is the light velocity in vacuum.

The left-hand side (LHS) of Eq. (1) is the acoustic wave equation while the right-hand side (RHS) of Eq. (1) is the optical beat that drives the acoustic wave through electrostriction. Although this equation describes stimulated Brillouin scattering in which both pump and Stokes are sent into the ONF, it can be used to identify the acoustic modes that will contribute to the spontaneous regime, which is described by Eq. (2). In this case, we take advantage of the fact that both regimes satisfy the phase-matching condition. Solving Eq. (1) without first identifying the most relevant acoustic modes is tedious because the number of acoustic modes is huge. So we first numerically solve Eq. (1) using a full-vectorial finite-element method (FEM) to get the displacement fields and the kinetic energy density. The simulations show that few acoustic modes contribute to the Brillouin backscattering. Those few resonances come from low-order longitudinal modes (referred to as L0x) and the torso-radial (TR) modes [17,18]. More details are provided in Supplement 1, Note 2.

By adding slight ellipticity to the fiber in the FEM simulation, we find that the TR21 acoustic mode becomes doubly degenerate. In our case, the two modes denoted TR21₊ and TR21_× show a frequency difference much smaller than the resonance linewidth. We also find that those two degenerated acoustic modes, the pump polarization, and the Stokes polarization are strongly correlated. The results are summarized in Table 1. (See Supplement 1, Note 3, for more details about the simulations).

Table 1. TR21 degenerated acoustic modes numerically computed from Eq. (1) for different pump and Stokes states of polarization (SOP).

\vec{H} = horizontal, \vec{V} = vertical.

Acoustic mode	Pump SOP	Stokes SOP
TR21 ₊	\vec{H}	$-\vec{H}$
TR21 ₊	\vec{V}	\vec{V}
TR21 _×	\vec{H}	\vec{V}
TR21 _×	\vec{V}	\vec{H}

A straightforward result from Table 1 is that in the context of spontaneous Brillouin scattering, a linearly polarized pump light will be scattered into two orthogonally polarized Stokes beams by the TR21₊ and the TR21_× modes, respectively. In the case of spontaneous Brillouin scattering, the acoustic waves come from thermal agitation and thus the TR21₊ and TR21_× waves are randomly phase-shifted. From this result and by using a Jones-Stokes-Mueller formalism, we can describe analytically the behavior of the state of polarization (SOP) of the Brillouin backscattered Stokes light, according to the SOP of the pump signal:

$$\vec{S}_s = M_{\text{TR21}} \vec{S}_p, \quad (3)$$

where $\vec{S}_s = (S_{s_0}, S_{s_1}, S_{s_2}, S_{s_3})$ and $\vec{S}_p = (S_{p_0}, S_{p_1}, S_{p_2}, S_{p_3})$ are the Stokes and pump SOPs defined by their four Stokes parameters and M_{TR21} is the Mueller SOP transformations matrix describing the polarization of the Stokes light scattered by the superposition of random phase shifted phonons TR21₊ and TR21_× [33]. Since the contribution of the two TR21₊ and TR21_× are indistinguishable and appear as a single resonance in the Brillouin spectrum we will denote it TR21.

To get a better insight, it is useful to compare our results with the Brillouin scattering coming from the acoustic longitudinal modes L0x that have no OAM. In the Brillouin spectrum, the

longitudinal resonances appear at different frequencies making the comparison quite easy. To get the L0x case, we switched the transformation matrix in Eq. (3) to a matrix denoted M_{L0x} . We then computed the Mueller matrices for both TR21 and L0x resonances using the convention of polarization coordinates independently from the wave propagation direction. (See complete calculations in [Supplement 1](#), Note 4). This yields:

$$M_{TR21} = \begin{pmatrix} 1 & 0 & 0 & 0 \\ 0 & 0 & 0 & 0 \\ 0 & 0 & 0 & 0 \\ 0 & 0 & 0 & -1 \end{pmatrix}, \quad M_{L0x} = \begin{pmatrix} 1 & 0 & 0 & 0 \\ 0 & 1 & 0 & 0 \\ 0 & 0 & 1 & 0 \\ 0 & 0 & 0 & 1 \end{pmatrix}, \quad (4)$$

Using the above matrices and Eq. (3), we calculated the theoretical SOP of the backscattered light, and the results are summarized in [Table 2](#) for both the L0x and TR21 resonances.

Table 2. Calculated longitudinal (L0x) and torso-radial (TR21) phonons generated Stokes SOPs for different pump SOPs. \vec{H} , \vec{V} , $\vec{+45^\circ}$, $\vec{-45^\circ}$, \vec{R} , \vec{L} , - stand for horizontal, vertical, diagonal at $+45^\circ$, -45° , right-hand and left-hand circular polarized light and unpolarized light, respectively. Note that with the chosen convention, the polarization frame does not change with propagation direction. Brillouin backscattered light (L0x) retains the same polarization state as the pump.

Pump SOP	\vec{H}	\vec{V}	$\vec{+45^\circ}$	$\vec{-45^\circ}$	\vec{R}	\vec{L}
L0x Stokes SOP	\vec{H}	\vec{V}	$\vec{+45^\circ}$	$\vec{-45^\circ}$	\vec{R}	\vec{L}
TR21 Stokes SOP	-	-	-	-	\vec{L}	\vec{R}

The mirror effect due to backscattering can be seen in the L0x matrix (Eq. (4)) since with the chosen polarization convention, the matrix of a mirror is the identity matrix. [Table 2](#), thus shows that longitudinal phonons (L0x) generate Stokes light that is perfectly polarized and the SOP from the pump is kept unchanged which is typical of Brillouin scattering in standard fibers [28]. Concerning the TR21 degenerated phonon, two specific cases arise depending on the pump SOP.

First, if the pump light is linearly polarized, the Stokes scattered light is depolarized as indicated by the - symbol. The superposition of two orthogonally polarized beams with random phase-shift leads to a scrambled polarization Stokes light, as observed in previous GAWBS experiments [34]. This is due to the fact that the columns in light yellow in Eq. (4) are all zeros. It comes from the incoherent superpositions of $TR21_+$ and $TR21_-$ that average to zero (see [Supplement 1](#), Note 4). The second case deals with circular polarizations that carry a spin angular momentum. When a circularly polarized pump wave \vec{L}/\vec{R} is launched into the ONF (spin $s = \pm 1$), the two $TR21_{+/-}$ contributions to the Brillouin scattering are such that the backscattered Stokes wave is fully polarized with an opposite circular polarization to the pump ($s = \mp 1$):

$$M_{TR21} \vec{L}/\vec{R} = \vec{R}/\vec{L} \quad (5)$$

In this specific case, the Stokes beam polarization is no longer scrambled. This has not been observed in GAWBS experiments but has recently been reported in chiral photonic crystal fibers [20]. Another way to explain this circular polarization-handedness inversion is to consider the two $TR21 \odot$ and $TR21 \ominus$ vortices modes with angular momentum ± 2 , as shown in [Fig. 1\(d\)](#) and [\(e\)](#).

They can be interpreted as an optomechanical spin-orbit interaction in which the orbital angular momentum (OAM) l of the acoustic vortices and spins of the pump and Stokes beams

(s_p and s_s) satisfy the conservation of total angular momentum (AM) $s_p = l + s_s$, in addition to the phase matching condition $\beta_p = \beta_a + \beta_s$ and the energy conservation $\omega_p = \omega_a + \omega_s$. Since the two optical pump and Stokes waves are circularly polarized, they respectively carry SAM of ± 1 [35]. On the acoustic side, a vortex with a topological charge l is similar to an l -order Bessel beam owning both spin and orbital AM. Considering the cylindrical symmetry of the waveguide, the integration of the spin density over a volume makes the spin contribution to the total integral AM of the beam vanishing ($\langle S \rangle = 0$). Consequently, the TR21 \odot and TR21 \ominus acoustic waves exhibit AM with a purely orbital character and the beams can be considered as acoustic vortices with azimuthal orders $l = \pm 2$. The angular momentum conservation law during Brillouin backscattering by the TR21 \odot and TR21 \ominus acoustic vortices is summarized in Table 3.

Table 3. Spin for pump (s_p), Stokes (s_s) and angular momentum AOM l for TR21 \odot and TR21 \ominus . For all the black lines total angular momentum conservation is respected, $s_p = l + s_s$. The red lines are excluded because total AM conservation is not possible (NA = not allowed).

Acoustic vortices	Pump spin (s_p)	TR21 OAM (l)	Stokes spin (s_s)
TR21 \odot	-1	-2	1
TR21 \odot	1	-2	NA
TR21 \ominus	-1	+2	NA
TR21 \ominus	1	+2	-1

One can see that the red lines are forbidden because the photon spin can only have a ± 1 value. For example, if right circularly polarized pump light ($s_p = 1$) interacts with a TR21 $\odot = \frac{1}{\sqrt{2}}$ (TR21₊ + iTR21_×) phonon, calculations show that both the TR21₊ and TR21_× contributions cancel each other, and thus there is no scattered light (see Supplement 1, Note 4). Note that in the experiments that will be presented in the following, we are not able to address a single TR21 \odot . However, this remarkable result is the reason why polarization scrambling disappears for a pump wave that is circularly polarized ($s_p = \pm 1$). Indeed, when incoherent contributions of both TR21 \odot and TR21 \ominus are present, any linear polarized pump light will interact with both acoustic vortices leading to a Stokes light with scrambled polarization. On the opposite, if circularly polarized pump light is sent, only one of the two TR21 \odot and TR21 \ominus will scatter light backward because of the angular momentum conservation shown in Table 3. As a result, the Stokes scattered light will be fully polarized with orthogonal polarization to the L0x modes scattered light as shown in Table 2. Note that in the context of spontaneous Brillouin scattering, the anti-Stokes process can be treated similarly.

3. Polarization-sensitive measurements

The experimental setup used for polarization-sensitive measurements of Brillouin scattering and observation of the spin-orbit coupling-induced circular polarization reversal is depicted in Fig. 2(a). We implemented a heterodyne detection technique from [18] for measuring the Brillouin backscattering combined with a polarization control and a polarimeter to observe the polarization dynamics. As a pump laser, we used a continuous-wave (CW) narrow-linewidth linearly-polarized DFB fiber laser at 1550 nm, which was sent to a motorized fiber polarization controller (MPC) to shape the input polarization state. It was then split using a directional fiber coupler (C1) into two beams. The top beam in pink serves as a pump for Brillouin backscattering, while the second beam in green is a reference beam or a local oscillator for heterodyne detection. The pump was then amplified using an erbium-doped fiber amplifier (EDFA) up to 33 dBm and transmitted to the silica nanofiber through an optical circulator (port 2). The nanofiber was made from a standard single-mode silica fiber (SMF-28) using the tapering technique described in

Ref. [18]. It has a diameter of 730 nm over a long uniform length of 10 cm. The Brillouin backscattered Stokes light from the ONF is then collected at port 3 (see blue arrow) and is mixed with the reference beam using a second fiber coupler (C2). The interference at the C2 output generates an optical beat signal that is further detected in the electrical domain using a fast photodiode. A polarimeter was placed on one of the two outputs of the coupler C2 to separately check the polarization states of the pump and reference signals. All fibers were maintained straight during the measurements to avoid any strain-induced polarization variation effects. The electrical signal was amplified and analyzed with an electrical spectrum analyzer (ESA), giving the Brillouin spectrum of the ONF, which is plotted in blue in Fig. 2(b).

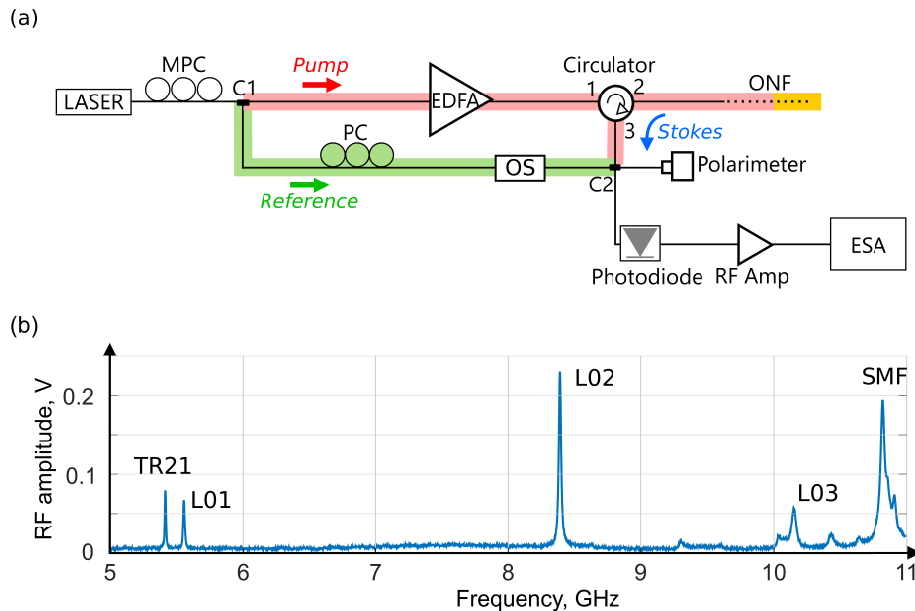


Fig. 2. (a) Schematic illustration of the polarization-sensitive BS detection set-up. MPC: Motorized Polarization Controllers; EDFA: erbium-doped fiber amplifier; ONF: optical nanofiber; PC: manual polarization controllers; OS: optical switch; RF Amp: radio-frequency amplifier; ESA: electrical spectrum analyzer. (b) Measured ONF Brillouin spectrum with Torso Radial TR21 acoustic mode, L01, and L02 longitudinal acoustic mode signatures. The nanofiber has a 730 nm diameter.

The two first peaks around 5.5 GHz are the Brillouin signals from the torso-radial and longitudinal acoustic modes (TR21 and L01 modes), while the third peak at 8.4 GHz comes from the hybrid acoustic L02 mode. The fourth main peak at 10.8 GHz is due to the single-mode fiber (SMF) in the all-fiber setup, as already shown in Ref. [18]. Peak amplitude is greatest when both the reference beam (green) and the backscattered light (Stokes, blue) share the same SOP leading to strong interference. On the other hand, if both SOPs are orthogonal, the blue peaks vanish. The heterodyne measurement thus makes it possible to project the Stokes beam SOP onto the reference beam SOP by measuring the peak amplitudes. A manual polarization controller (PC) was added to the reference arm to control this projection (see Supplement 1, Note 5). However, when the pump SOP is varied using the MPC, the reference beam SOP also varies due to the non-polarization maintaining fibers used in the setup. To minimize this effect, we adjust the polarization controller (PC) to maximize, for any given pump SOP, the interference between the reference beam and a beam that propagates along the pink path and is reflected at the cleaved output of the ONF (orange). This beam travels the same path as the Brillouin backscattered

light, except for the orange path. Further details about the method are given in [Supplement 1](#), Note 6. This setting allows us to compensate for any polarization rotation between the green and pink-orange paths. Since Brillouin scattering from a longitudinal wave does not change the state of polarization [28], the amplitude of the hybrid acoustic wave (with both pressure and shear components) peak such as the L02 should be maximum whatever the SOP produced at the output of the MPC controller. This can be verified in Fig. 3 which shows various Brillouin spectra centered at the L02 mode frequency for six different input pump SOPs, pointed by a color marker on the Poincaré sphere. We note in Fig. 3 that the amplitude of the L02 peak is constant and independent of the pump SOP configuration. This indicates the effectiveness of our method for the alignment of the two optical paths.

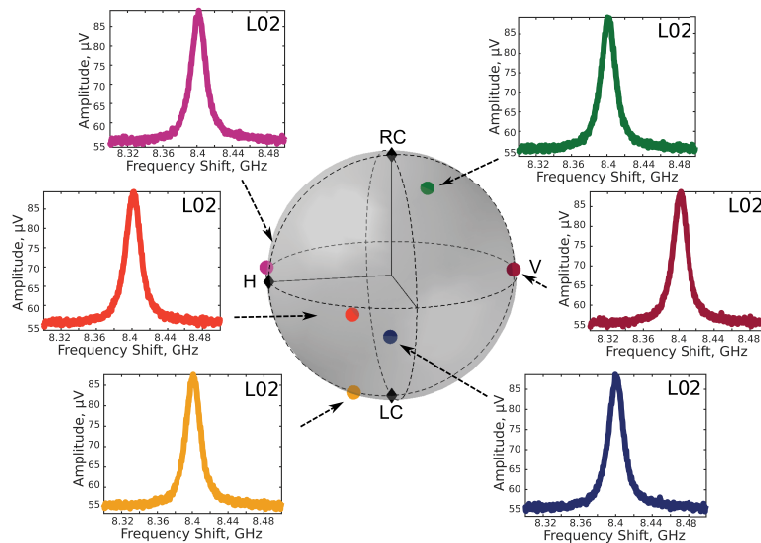


Fig. 3. Experimental Brillouin spectra of the L02 acoustic mode resonance at 8.4 GHz from a 730 nm diameter silica nanofiber as a function of the input pump polarization indicated on the Poincaré sphere.

4. Experimental results

With our setup, it is possible to go through several pump polarization states while projecting the SOP of the Stokes light onto the SOP of the pump. We, therefore, carried out the same experiment as before, this time reproducing the measured amplitude of the TR21 peak in false color, as shown in Fig. 4(a) for each pump SOP on the Poincaré sphere. We can clearly observe an equatorial belt of higher intensity in red compared to the two poles of minimum intensity (blue). The two markers on the sphere point to the spectra from the measurements for maximum (red, top) and minimum (blue, bottom) intensities.

This confirms that, unlike the L02 mode, the TR21 mode strongly affects the polarization of the Stokes wave. To interpret these results, we simulated the polarization dynamics on the sphere with the model introduced in the theoretical section. The numerical simulation is presented in Fig. 4(b). As can be seen, we see as in the experimental figure a red equatorial belt delimited by black dashed lines. This corresponds to the area surrounding the linear polarization of the pump beam which gives rise to depolarized backscattered waves. Note that the blue color in Fig. 4(b) corresponds to a zero beating intensity, as the reference and TR21 Stokes waves are cross-polarized, and the red color matches with the 0.5 averaged intensity between the fully polarized reference wave and the depolarized TR21 Stokes wave. Note also that the rotation

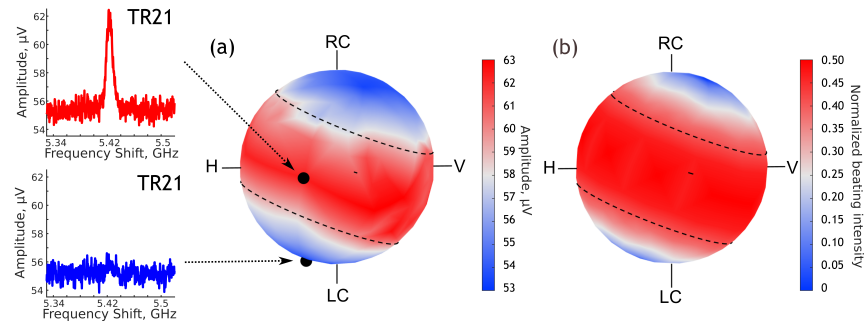


Fig. 4. Polarization state dynamics of the TR21-mode induced Brillouin backscattering. Experimental (a) and numerical (b) TR21 peak intensity represented in false color on the Poincaré sphere describing the pump SOP. The two experimental spectra are extracted for the pump SOPs indicated with black markers.

of the poles with respect to the displayed reference frame (H,V,RC,LC) is due to the evolution of the Brillouin SOP between the center of the ONF and the polarimeter [36]. To validate this interpretation, we fixed the pump polarization with a linear SOP, as depicted by the red marker in Fig. 5 on the Poincaré sphere. The polarization of the reference beam was then rotated and we measured several Brillouin spectra, which are shown in grey in Fig. 5. On the right, the L02 peak near 8.4 GHz goes from a maximum intensity (pink) when the reference beam is co-polarized with the L02 Stokes wave to a near-zero minimum (green) when the reference wave is cross-polarized. We measured a high polarization extinction ratio (PER) of ≈ 14 dB, which confirms that the Brillouin Stokes wave backscattered by the L02 mode is well polarized. Conversely, we can clearly see in Fig. 5 that there is almost no significant change in the Brillouin peak amplitude at 5.43 GHz due to the TR21 mode. The PER can be neglected (≈ 0 dB). The TR21 peak is therefore insensitive to the polarization of the reference wave, which confirms the depolarization of the TR21 Stokes wave.

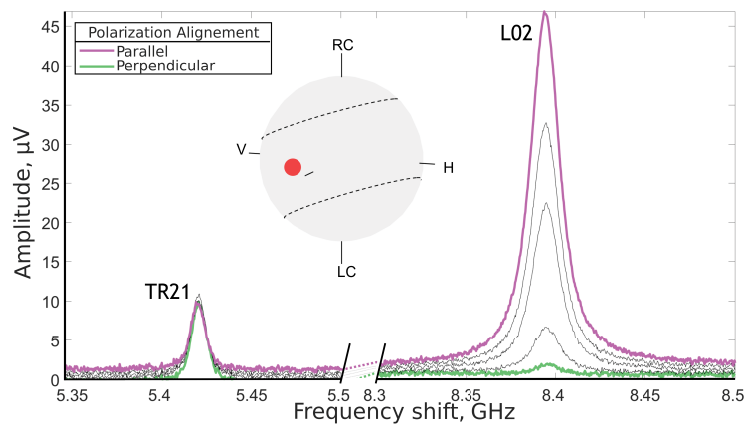


Fig. 5. Experimental Brillouin spectra of the TR21 and L02 modes for different polarizations of the reference beam. The linear pump SOP is depicted on the Poincaré sphere as a red dot and the reference beam polarization varies between parallel and perpendicular SOP. The TR21 signal appears depolarized.

Since the linear polarization of the pump corresponds to the red belt in Fig. 4, the blue poles are associated with the right-handed (RC) and left-handed (LC) circular polarizations, respectively.

The blue areas on the Poincaré sphere thus reveal a TR21 peak close to zero, as shown by the blue spectrum on the left of Fig. 4, due to the absence of interference with the reference wave. This is only possible if the backscattered TR21 signal is fully polarized and its SOP is orthogonal to the pump SOP. Consequently, a left-handed circularly polarized pump wave will be backscattered into a right-handed circularly polarized Brillouin Stokes wave and vice versa. This is consistent with the theoretical results presented in Table 3 and this is due to the conservation of total angular momentum, which implies that the spin of the pump light couples with the orbital momentum of the acoustic vortex TR21 mode to generate a backscattered signal with a spin opposite to that of the pump wave.

To further validate our model, we then fixed the pump SOP on one of the blue poles (right circular polarization) of the Poincaré sphere, as shown by the black dot in Fig. 4(a). It is also depicted as a red dot in Fig. 6. We performed the same measurements as before by varying the polarization of the reference beam and measuring the Brillouin spectra for the TR21 and the L02 modes, respectively. Results are shown in Fig. 6. The L02 peak shows similar high polarization-sensitivity, as in Fig. 5, with an extinction ratio close to 14 dB. However, unlike the previous measurement, the TR21 now appears to be highly sensitive to reference beam polarization. Indeed, peak amplitude is observed with the green curve while the peak is almost removed with the green curve, and the PER is as high as 10 dB. This confirms that the TR21 Stokes wave is well polarized and leads to strong interference. It is worth noting that the maximum amplitude TR21 peak in Fig. 6 is ≈ 3 dB higher than the TR21 peak in Fig. 5. Indeed, when the signal is fully polarized, the optical beat amplitude is maximized, whereas the average beat amplitude is only 0.5 when the TR21 signal is depolarized. We can also clearly see in Fig. 6 that, when the TR21 peak is maximal, the L02 peak is minimal and vice versa, meaning that the pump and Stokes waves are cross-polarized. Since the pump wave is circularly polarized, this implies that, due to the conservation of angular momentum, a left/right-hand circularly polarized optical pump wave is backscattered into a right/left-hand circularly polarized Stokes light when interacting with an acoustic TR21 vortex wave with a topological charge of order ± 2 .

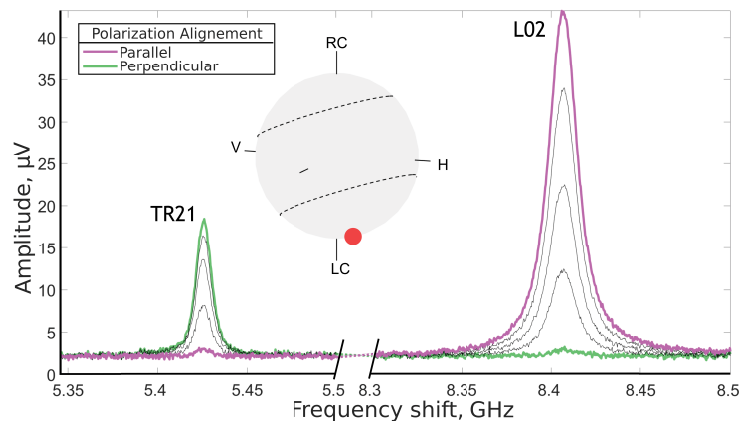


Fig. 6. Polarization sensitive Brillouin TR21 backscattered signal. The pump SOP is circular and depicted on the Poincaré sphere and the reference polarization varies between parallel and perpendicular SOP. The TR21 signal shows a polarization dependence.

5. Conclusion

In this work, we theoretically and experimentally investigated the polarization properties of the backward Brillouin scattering in an optical nanofiber, with special attention to the torso-radial vortex TR21 acoustic mode that carries angular orbital momentum. We predicted and observed

two different dynamics depending on the polarization state of the pump beam. On one hand, when the pump beam is linearly polarized, the superposition of the incoherent contributions of the doubly degenerated $TR21_+$ and $TR21_×$ modes induces a strong depolarization of the backscattered Stokes beam. On the other hand, when the pump beam is circularly polarized and thus carries a spin angular momentum (± 1), a spin-orbit interaction takes place and the angular momentum conservation implies that the backscattered Brillouin signal exhibits an opposite spin, and thus a handedness circular polarization reversal. Those two regimes were modeled using a full-vectorial FEM of the optoacoustic interaction and then confirmed by experimental polarization-sensitive measurements with very good agreement. The observation of this optomechanical spin-orbit coupling-induced circular polarization inversion is particularly reminiscent of Beth's historical experiment, while still finding great potential for future applications for all-optical information processing, all-optical memories, or in the development of non-reciprocal photonic components such in-fiber isolators.

Funding. EIPHI Graduate School (ANR-17-EURE-0002); Conseil régional de Bourgogne-Franche-Comté; SupMicrotech-ENSMM.

Acknowledgements. The authors thank Jacques Chretien, Camille Buret, and Martin Hauden for their contribution to this work and Xinglin Zeng for helpful discussions.

Disclosures. The authors declare no conflicts of interest.

Data availability. Data underlying the results presented in this paper are not publicly available at this time but may be obtained from the authors upon reasonable request.

Supplemental document. See [Supplement 1](#) for supporting content.

References

1. K. Y. Bliokh, F. J. Rodríguez-Fortuño, F. Nori, and A. V. Zayats, "Spin-orbit interactions of light," *Nat. Photonics* **9**(12), 796–808 (2015).
2. A. Aiello, P. Banzer, M. Neugebauer, and G. Leuchs, "From transverse angular momentum to photonic wheels," *Nat. Photonics* **9**(12), 789–795 (2015).
3. J. H. Poynting, "The Wave Motion of a Revolving Shaft, and a Suggestion as to the Angular Momentum in a Beam of Circularly Polarised Light," *Proceedings of the Royal Society of London Series A* **82**, 560–567 (1909).
4. R. A. Beth, "Mechanical Detection and Measurement of the Angular Momentum of Light," *Phys. Rev.* **50**(2), 115–125 (1936).
5. M. Padgett and R. Bowman, "Tweezers with a twist," *Nat. Photonics* **5**(6), 343–348 (2011).
6. D. Hakobyan and E. Brasselet, "Left-handed optical radiation torque," *Nat. Photonics* **8**(8), 610–614 (2014).
7. E. F. Fenton, A. Khan, P. Solano, L. A. Orozco, and F. K. Fatemi, "Spin-optomechanical coupling between light and a nanofiber torsional mode," *Opt. Lett.* **43**(7), 1534–1537 (2018).
8. D. Su, P. Solano, J. D. Wack, L. A. Orozco, and Y. Zhao, "Torsional optomechanical cooling of a nanofiber," *Photonics Res.* **10**(2), 601–609 (2022).
9. S. Franke-Arnold, "Optical angular momentum and atoms," *Philos. Trans. R. Soc., A* **375**(2087), 20150435 (2017).
10. M. Wang, H. Zhang, T. Kovalevich, R. Salut, M.-S. Kim, M. A. Suarez, M.-P. Bernal, H.-P. Herzig, H. Lu, and T. Grosjean, "Magnetic spin-orbit interaction of light," *Light: Sci. Appl.* **7**(1), 24 (2018).
11. M. Onoda, S. Murakami, and N. Nagaosa, "Hall effect of light," *Phys. Rev. Lett.* **93**(8), 083901 (2004).
12. O. Hosten and P. Kwiat, "Observation of the Spin Hall Effect of Light via Weak Measurements," *Science* **319**(5864), 787–790 (2008).
13. L. Marrucci, C. Manzo, and D. Paparo, "Optical spin-to-orbital angular momentum conversion in inhomogeneous anisotropic media," *Phys. Rev. Lett.* **96**(16), 163905 (2006).
14. S. Wang, G. Zhang, X. Wang, Q. Tong, J. Li, and G. Ma, "Spin-orbit interactions of transverse sound," *Nat. Commun.* **12**(1), 6125 (2021).
15. K. Y. Bliokh and F. Nori, "Spin and orbital angular momenta of acoustic beams," *Phys. Rev. B* **99**(17), 174310 (2019).
16. L. Tong, R. R. Gattass, J. B. Ashcom, S. He, J. Lou, M. Shen, I. Maxwell, and E. Mazur, "Subwavelength-diameter silica wires for low-loss optical wave guiding," *Nature* **426**(6968), 816–819 (2003).
17. J.-C. Beugnot, S. Lebrun, G. Pauliat, H. Maillotte, V. Laude, and T. Sylvestre, "Brillouin light scattering from surface acoustic waves in a subwavelength-diameter optical fibre," *Nat. Commun.* **5**(1), 5242 (2014).
18. A. Godet, A. Ndao, T. Sylvestre, V. Pecheur, S. Lebrun, G. Pauliat, J.-C. Beugnot, and K. P. Huy, "Brillouin spectroscopy of optical microfibers and nanofibers," *Optica* **4**(10), 1232–1238 (2017).
19. X. Zeng, P. S. Russell, C. Wolff, M. H. Frosz, G. K. L. Wong, and B. Stiller, "Nonreciprocal vortex isolator via topology-selective stimulated Brillouin scattering," *Sci. Adv.* **8**(42), eabq6064 (2022).

20. X. Zeng, W. He, M. H. Frosz, A. Geilen, P. Roth, G. K. L. Wong, P. S. J. Russell, and B. Stiller, "Stimulated Brillouin scattering in chiral photonic crystal fiber," *Photonics Res.* **10**(3), 711–718 (2022).
21. X. Zeng, P. S. J. Russell, Y. Chen, Z. Wang, G. K. L. Wong, P. Roth, M. H. Frosz, and B. Stiller, "Optical vortex Brillouin laser," arXiv, arXiv 2204.11971 (2022).
22. P. Z. Dashti, F. Alhassen, and H. P. Lee, "Observation of Orbital Angular Momentum Transfer between Acoustic and Optical Vortices in Optical Fiber," *Phys. Rev. Lett.* **96**(4), 043604 (2006).
23. H. H. Diamandi, G. Bashan, Y. London, K. Sharma, K. Shemer, and A. Zadok, "Interpolarization Forward Stimulated Brillouin Scattering in Standard Single-Mode Fibers," *Laser Photonics Rev.* **16**(1), 2100337 (2022).
24. G. Bashan, H. H. Diamandi, Y. London, K. Sharma, K. Shemer, E. Zehavi, and A. Zadok, "Forward stimulated Brillouin scattering and opto-mechanical non-reciprocity in standard polarization maintaining fibres," *Light: Sci. Appl.* **10**(1), 119 (2021).
25. A. P. Greenberg, Z. Ma, and S. Ramachandran, "Angular momentum driven dynamics of stimulated Brillouin scattering in multimode fibers," *Opt. Express* **30**(16), 29708 (2022).
26. M. Merklein, B. Stiller, K. Vu, S. J. Madden, and B. J. Eggleton, "A chip-integrated coherent photonic-phononic memory," *Nat. Commun.* **8**(1), 574 (2017).
27. B. Stiller, M. Merklein, C. Wolff, K. Vu, P. Ma, S. J. Madden, and B. J. Eggleton, "Coherently refreshing hypersonic phonons for light storage," *Optica* **7**(5), 492–497 (2020).
28. R. M. Shelby, M. D. Levenson, and P. W. Bayer, "Guided acoustic-wave Brillouin scattering," *Phys. Rev. B* **31**(8), 5244–5252 (1985).
29. F. Lei, G. Tkachenko, J. M. Ward, and S. Nic Chormaic, "Complete Polarization Control for a Nanofiber Waveguide Using Directional Coupling," *Phys. Rev. Appl.* **11**(6), 064041 (2019).
30. J.-C. Beugnot and V. Laude, "Electrostriction and guidance of acoustic phonons in optical fibers," *Phys. Rev. B* **86**(22), 224304 (2012).
31. N. M. Kroll, "Excitation of Hypersonic Vibrations by Means of Photoelastic Coupling of High-Intensity Light Waves to Elastic Waves," *J. Appl. Phys.* **36**(1), 34–43 (1965).
32. V. Laude and J.-C. Beugnot, "Lagrangian description of Brillouin scattering and electrostriction in nanoscale optical waveguides," *New J. Phys.* **17**(12), 125003 (2015).
33. S. N. Savenkov, "Jones and Mueller matrices: structure, symmetry relations and information content," in *Light Scattering Reviews 4*, A. A. Kokhanovsky, ed. (Springer Berlin Heidelberg, Berlin, Heidelberg, 2009), pp. 71–119.
34. N. Nishizawa, S. Kume, M. Mori, T. Goto, and A. Miyauchi, "Experimental analysis of guided acoustic wave Brillouin scattering in PANDA fibers," *J. Opt. Soc. Am. B* **12**(9), 1651–1655 (1995).
35. K. Y. Bliokh and V. D. Freilikher, "Polarization transport of transverse acoustic waves: Berry phase and spin Hall effect of phonons," *Phys. Rev. B* **74**(17), 174302 (2006).
36. M. Joos, A. Bramati, and Q. Glorieux, "Complete polarization control for a nanofiber waveguide using the scattering properties," *Opt. Express* **27**(13), 18818–18830 (2019).